JOURNAL OF AIRCRAFT
Vol. 35, No. 1, January–February 1998

Shape Optimizing Nacelle near Flat-Plate Wing Using Multiblock Sensitivity Analysis

Mohamed E. Eleshaky* and Oktay Baysal†
Old Dominion University, Norfolk, Virginia 23529

A major design task in reducing the overall aircraft drag is the integration of the engine nacelles and the airframe. With this impetus, a methodology was demonstrated to optimize nacelle shapes with and without the presence of a flat-plate nearby to account for the wing interference. Overly simplified shapes notwithstanding, this process requires multiblock grids not only for its aerodynamic analysis, but also for its optimization. Although the former is a standard practice, the latter has only recently been possible for the gradient-based optimizations with the development of the sensitivity analysis with domain decomposition scheme. The analyses were obtained by solving the three-dimensional, compressible, thin-layer Navier–Stokes equations using an implicit, upwind-biased, finite volume scheme. In addition to demonstrating the present method's suitability for automated shape optimization of interfering aircraft components, such as a nacelle and a wing, the results verified two important issues. First, accounting for the aerodynamic mutual interference between components in close proximity manifested itself in a shape different than that obtained when a component was assumed to be isolated. Secondly, even for isolated-component designs, neglecting the viscous effects compromised not only the flow physics but also the optimized shapes.

Nomenclature

C_D = drag coefficient
C_p = pressure coefficient
d_i, d_o = nacelle's inlet and outlet diameters
F = objective function
G = constraint
nbl = number of subdomains around design surfaces
Q = conserved flow variables
R = residual form of conservation equations
t = nacelle thickness
X_D = design variable
$\boldsymbol{\lambda}$ = adjoint vector

Subscripts
f = flow type
g = geometric type
j, m = dummy indices

Superscripts
b = boundary cell
i = internal cell
k = kth subdomain
T = transpose

Introduction

THE recent resurgence of interest in a supersonic transport has initially targeted the prerequisite of reducing aircraft drag and associated environmental noise levels. One of the major tasks in designing such an aircraft is minimizing the installed-nacelle-induced drag. By studying the flowfield of the integrated nacelle and wing, as opposed to those of isolated components, a designer can exploit favorable interference effects in achieving minimized overall drag.[1] Many concepts, such as favorable interference and wing reflexing,[2] have been used in design practice for many years. The wing reflexing, for example, has been demonstrated[3] by using a modified linearized potential method, where the viscous and other nonlinear aerodynamic effects have not been taken into account. As a remedy, Navier–Stokes calculations[4] have recently been performed to provide the required data for a quasi-empirical correction of this method. Further Navier–Stokes computations were performed to study two types of domain decomposition methods in analyzing the flowfield of a wing/body/nacelle/diverter assembly.[5] However, these efforts generated only a matrix of analyses, which conceivably could be used in a cut-and-try type design effort or for the corrections of the linear methods.

With the recently developed gradient-based methods[6,7] (ADOS, aerodynamic design optimization with sensitivities), as will be demonstrated as a proof-of-concept in this paper, it is now possible to optimize the nacelle integration based on nonlinear analyses and in an automated manner. The connective role of sensitivity analysis[6,7] within such methods was shown to be a key element in the automatic shaping of aerodynamic surfaces[8] and resulted in tremendous savings in the computational cost. To extend the applicability of these methods to optimize surfaces of complex and multicomponent configurations, a three-dimensional scheme for sensitivity analysis using domain decomposition (SADD)[9,10] was also developed. Decomposing the computational domain into subdomains not only eased the grid generation task for the analyses, depending on the block and interface sizes, it also reduced the computer memory required for performing the sensitivity analysis. The present results demonstrated the first shape optimization of a three-dimensional and multiple-component configuration using a constrained and gradient-based approach.

Definition of Optimization Problems

It was desired to optimize the shape of a nacelle[11] surface (Fig. 1) to yield a minimized drag coefficient. The inner cross-sectional area of the quarter-nacelle was used as the reference area (0.19635 in.^{2}). Note that the reference area used in com-

Received March 7, 1994; revision received April 28, 1997; accepted for publication June 24, 1997.

*Research Associate, Mechanical Engineering and Mechanics Department; currently Assistant Professor, Mechanical Engineering Department, University of Alexandria, Alexandria 21544, Egypt. Member AIAA.

†Eminent Scholar and Professor, Aerospace Engineering Department. Associate Fellow AIAA.

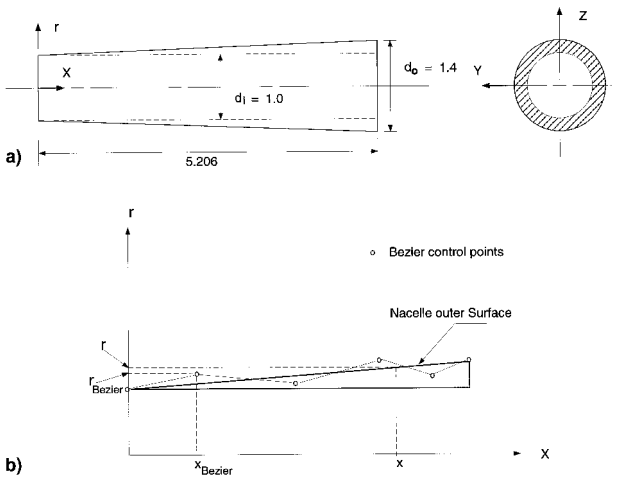

Fig. 1 Nacelle and flat-plate wing model for a supersonic transport vehicle[11]: (a) isolated nacelle and b) Bezier–Bernstein surface parameterization (all dimensions are in inches).

puting the propulsion drag is often the wing reference area; for example, assuming four engines, the reference area for a supersonic transport[11] would be 2.602 ft^2. For the sake of simplicity the surface of the nacelle was parameterized by a Bezier–Bernstein representation based on a fifth-degree Bernstein polynomial.[8] The first and the last control points were fixed and the radial coordinates of the remaining four control points (Fig. 1) were used as the design variables. This allowed a radial shape variation along each axial point, but restricted the circumferential variations. For the circumferential variations to be included, the bidirectional Bezier–Bernstein representation[12] would be needed.

Four idealized cases were performed to satisfy the objectives of the present proof-of-concept study. In cases 1 and 2, the axisymmetric nacelle was isolated from the flat-plate and the diffusion was neglected. Then, the outer surface of the nacelle shown in Fig. 1 was arbitrarily perturbed to two distinctly different shapes, which served as the initial shapes for two independent optimization cases. The motivation for cases 1 and 2 was to establish the accuracy of the methodology if both cases converged to the same final shape. In the third case, the viscous effects were included in optimizing the isolated nacelle shape and the flow was assumed to be laminar. The final case (case 4) was the optimization of the nacelle when it was brought near a flat-plate (representing the wing), with the inlet of the nacelle 13.5 in. downstream of the flat-plate leading edge. The nacelle centerline was located 1 in. from the flat-plate, and their longitudinal center planes were aligned (Fig. 1). The diffusion was again neglected in case 4. For computational savings, the aft-cowl of the nacelle and the diverter connecting the nacelle and the flat-plate were not included in the present configuration. The motivations for cases 3 and 4 were identifying the effects of viscosity and wing interference, respectively, on the optimized shapes.

The geometric constraints were posed to ensure that 1) t/d_i was positive and finite; 2) t/d_i was less than a specified value so that the nacelle/flat-plate clearance was finite; 3) nacelle's leading-edge slope was within specified values; 4) t_{inlet} and t_{base} were zero and a specified value, respectively; and 5) d_i and and d_o remained unchanged during the optimization (hence, constant inlet and base areas).

This optimization problem was mathematically represented as the minimization of an objective $F[Q(X_D), X_D]$, subject to the constraints $G_j[Q(X_D), X_D]$, where $j = 1, \text{NCON}_g$ (NCON is the number of constraints). The design variables were bounded by specified lower and upper limits $X_{D_m}^{\text{lower}}$ and $X_{D_m}^{\text{upper}}$ (side constraints), where $m = 1$, NDV (NDV is the number of design variables). For a multiblock approach, where the computational domain was divided into NBL subdomains, where NBL indicates the total number of blocks, the objective function needed to be the sum of the possible contributions from all NBL. However, because F in the present cases represented the drag, it depended only on the flowfield solution of the computational cells adjacent to the aerodynamic surfaces. Hence, the summation needed to be carried over only the nbl subdomains containing the nacelle and the flat-plate:

$$F[Q(X_D), X_D] = \sum_{k=1}^{nbl} F[Q_k(X_D), X_D] \tag{1}$$

The optimization problem was solved with the method of feasible directions, as implemented in the extensively validated computer code ADS (algorithm for design synthesis),[13] and using the ADOS (aerodynamic design optimization with sensitivities) procedure explained and validated in Refs. 6–8. An important ingredient of that procedure is the analytical determination of the sensitivity coefficients, which are the gradients of the objective function and the constraints with respect to the design variables. This feature is briefly discussed in the next section.

Flowfield and Sensitivity Analyses

The analysis equations used in this study were the three-dimensional, thin-layer Navier–Stokes equations for a laminar flow. However, for the inviscid cases, the diffusion terms were dropped, resulting in the Euler equations. Their discrete residual form was written in terms of the design variables and conserved flow variables, $R[Q(X_D), X_D]$.[6]

Among the two available methods for the sensitivity coefficients using a discrete approach,[6] the adjoint variable method was deemed more suitable for this study. This was because the number of design variables (NDV = 4) was greater than the number of adjoint variables ($\text{NCON}_f + 1 = 1$). Accordingly, the sensitivity coefficients were written in the domain decomposition form[9,10]:

$$\nabla F \equiv \frac{\partial F}{\partial X_D} = \left(\frac{\partial F}{\partial X_D}\right)_Q + (\boldsymbol{\lambda}^b)^T \cdot \left(\frac{\partial R^b}{\partial X_D}\right) + \sum_{k=1}^{\text{NBL}} \left[(\boldsymbol{\lambda}^i)^T \cdot \left(\frac{\partial R^i}{\partial X_D}\right)\right]^k \tag{2}$$

The adjoint vectors $\boldsymbol{\lambda}^i$ and $\boldsymbol{\lambda}^b$ were obtained using the preconditioned SADD scheme[10] developed to solve a nonsymmetric, sparse system of linear equations that could be symbolically represented as follows:

$$\begin{bmatrix} \left[\left[\frac{\partial R^i}{\partial Q^i}\right]^T\right]^k & \left[\left[\frac{\partial R^b}{\partial Q^i}\right]^T\right]^k \\ \left[\left[\frac{\partial R^i}{\partial Q^b}\right]^T\right]^k & \left[\frac{\partial R^b}{\partial Q^b}\right]^T \end{bmatrix} \begin{Bmatrix} \{\boldsymbol{\lambda}^i\}^k \\ \{\boldsymbol{\lambda}^b\} \end{Bmatrix} = \begin{bmatrix} \left[\frac{\partial F}{\partial Q^i}\right]^k \\ \frac{\partial F}{\partial Q^b} \end{bmatrix}$$

$$k = 1, \text{NBL} \tag{3}$$

When the axisymmetric nacelle was isolated and positioned at zero yaw and angle of attack, only a quarter of the nacelle needed to be considered. The composite grid for the nacelle contained 16 H–O type multiblock grids (NBL = 16) with proper clustering of points near the solid surfaces (Fig. 2). One of these blocks discretized inside of the nacelle and was used in computing the through-flow. However, when the nacelle was placed near the flat-plate, again at zero yaw and angle of attack, the symmetry was with respect to the longitudinal center plane only, which required considering one-half of the configuration (Fig. 1). Then, the composite grid consisted of 21 H–O type multiblock grids (NBL = 21). Depending on the case, there were between 16,000 and 21,000 cells in these blocks.

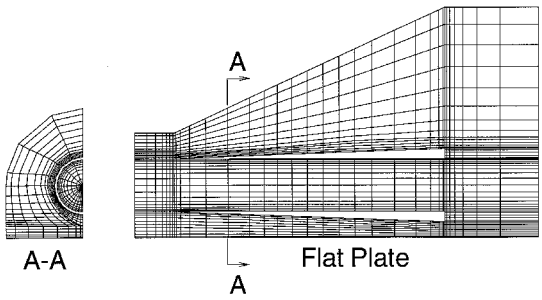

Fig. 2 Computational grid: longitudinal center plane and a cross section of the composite grid.

The computer code CFL3D (Ref. 14) was used to solve the flowfield equations by a finite volume, upwind-biased, alternating direction implicit (ADI) method. For the interior points and block interfaces, the method was conservative and at least second-order accurate spatially and first-order accurate temporally. The time term was used as a relaxation parameter to achieve convergence to the steady state with the L_2 norm of the residual R driven to about 1E−9 using local time stepping. The accuracy of this flow solver has been validated numerous times and reported in the literature,[4–10,13] hence, it will not be repeated herein.

All of the boundary conditions were specified explicitly. On solid surfaces, the impermeable wall, zero normal gradient of pressure, and adiabatic wall conditions were imposed. The no-slip condition for the viscous case and the tangency condition for the inviscid cases were also imposed on the solid surfaces. One-dimensional characteristic conditions were used for the outer boundaries. Reflection conditions were imposed on all planes of symmetry. Across the grid interfaces of the blocked grids, the gradients of the flow variables were transferred conservatively. At the upstream boundary, the freestream conditions were specified as follows: Mach number of 2.4, unit Reynolds number of 1.67E5 per inch, and total temperature of 585°R.

Results and Discussion

The results of each of the four cases investigated were illustrated by plotting the optimization histories of the nacelle shape, objective function (drag coefficient), design variables (Bezier control points), and surface pressure coefficients. In these figures, an iteration refers to a univariate search iteration, that is, without a sensitivity coefficient update. This is also known as the inner-loop iteration as opposed to an outer-loop iteration, which updates the sensitivities (search direction change).

In cases 1 and 2, the initial C_D values were 0.3433 and 0.3577, respectively. Starting with these initial shapes, two independent optimization cases were performed. The optimized shapes obtained (Fig. 3) were almost identical and the objective function values were equal to the fourth significant digit (0.2708); that is, the final optimized shape was virtually independent of the initial shape. Thus, the accuracy of the present methodology was established for the problem at hand. Because the alpha-step size[6,9] used in the univariate searches of the second optimization case was kept conservatively low (1E−3), the optimized shape was obtained after a relatively large number (405) of iterations, including three sensitivity updates. In retrospect, larger steps could have been used to achieve the same result. The optimization histories for the second isolated nacelle case are shown in Fig. 4. The shape was changed from a bell-type curve (because an arbitrary shape was aerodynamically not sensible) to almost a conical curve, essentially with the changes in the second and third design variables. This was explained with the help of the surface C_p distribution history. The initial shape caused a large expansion toward the base of the nacelle. To match the base pressure, a

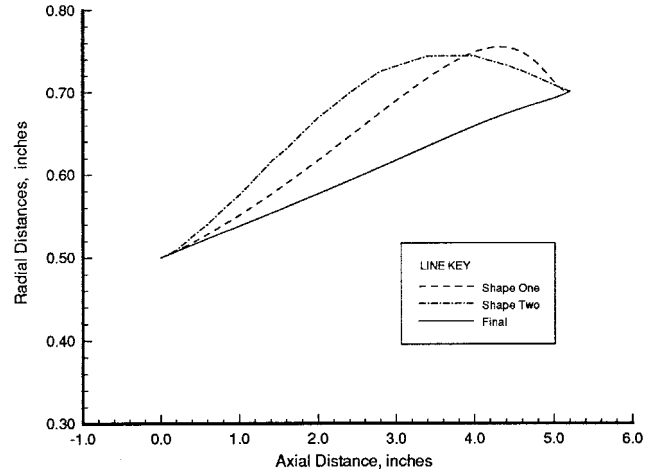

Fig. 3 Comparison of final isolated nacelle shapes, which started with different initial shapes, in inviscid flow (cases 1 and 2).

shock occurred near the outer base corner, resulting in an increased drag value (wave drag). Then, to minimize the drag, the optimizer reduced the surface curvature to weaken the shock, and it generated much smaller peak pressure magnitudes.

In optimizing the isolated nacelle by including the diffusion terms, the alpha-step size was quickly and linearly increased from 1E−3 to 5E−1. The optimized shape was obtained after 31 iterations, including three sensitivity updates. The initial total drag coefficient was 0.9658, and the optimization resulted in its reduction by about 16% (Fig. 5a). As a result of the optimization, the arbitrarily selected and highly convex initial curve became a concave one (Fig. 5b). Although the fourth design variable was also active, the main changes were dictated by the second and third design variables (Fig. 5c). The main reason for the shape to become concave was the effort of the optimization to reduce the wave drag caused by the leading-edge shock, as could be discerned from the surface C_p distributions (Fig. 5d). Interestingly, the shape continued to evolve after 12 iterations, despite no detectable changes in the total drag. A closer inspection of the optimization history indicated that there were violated constraints sporadically spread between iterations 12 and 25, but all constraints were satisfied at the end (final shape in the feasible region[12]). Note that, because the total wetted area did not change significantly, the skin friction drag remained virtually unchanged.

As the fourth case, the nacelle shape was optimized with the flat-plate nearby. The conical shape shown in Fig. 1 was used as the initial shape without any perturbations, with the initial C_D value being 0.2562. The optimization histories of the objective function, shape, and design variables are presented in Fig. 6. With the alpha-step size rapidly varied from 1.0E−2 to 1.4E−1, the optimization required 50 optimization iterations, including six sensitivity updates. Evidently, this shape did not reside in the feasible region defined by the present constraints. Hence, for the first 20 iterations, the optimizer changed the first three design variables (Fig. 6a), then the shape (Fig. 6b), to satisfy the constraints, but without any regard to the changes in the objective function (Fig. 6c). The shape became more convex and caused a stronger shock and higher wave drag. This was also evident in the history of the C_p distribution on the nacelle's bottom surface (Fig. 7a). After all of the constraints were satisfied, the optimizer started to decrease the convexity, which in turn reduced the shock strength and the wave drag. All of the design variables were varied during the optimization process (Fig. 6a). The final shape satisfied all of the constraints and offered a 5% drag reduction. Note that, unlike the previous cases, this was a reduction from an aerodynamically acceptable shape (cf. case 2 and Ref. 11). The C_p distribution history on the top centerline

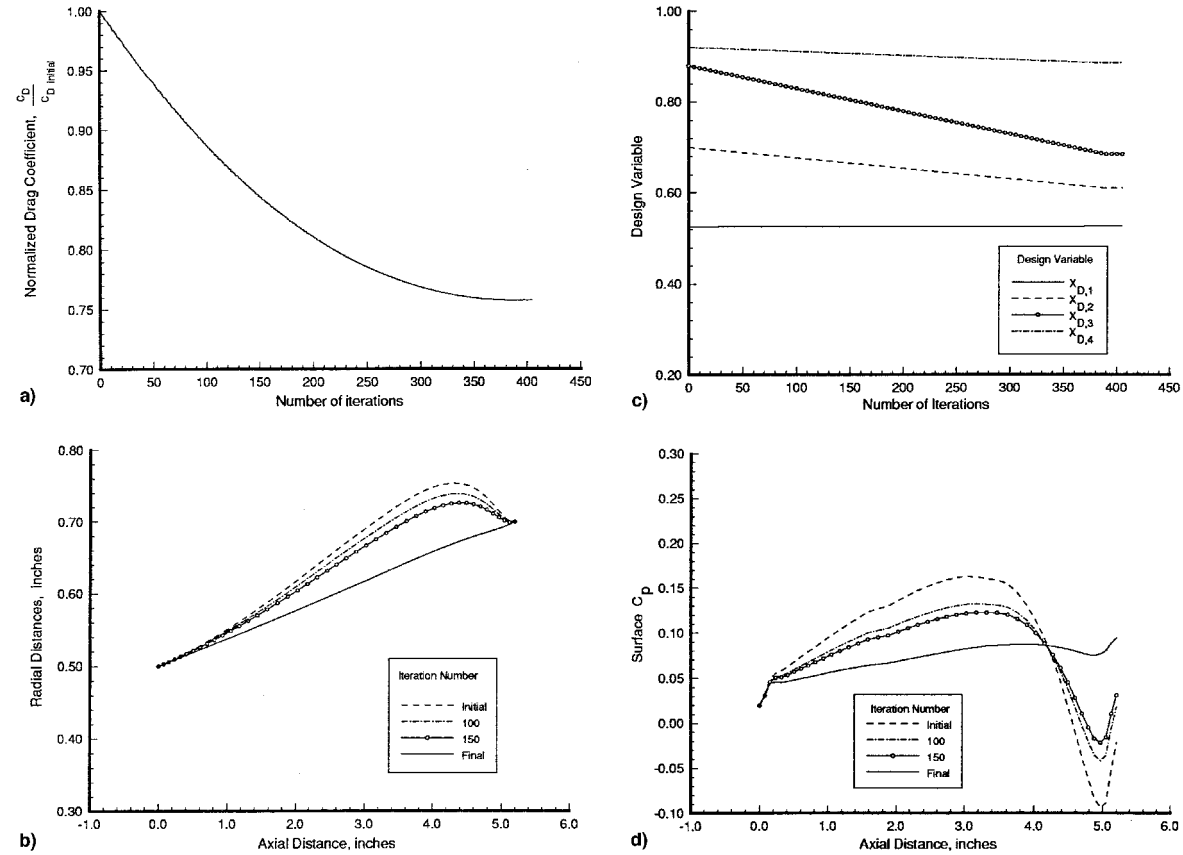

Fig. 4 Optimization of the isolated nacelle in inviscid flow (case 2): a) objective function history, b) shape evolution, c) history of design variables, and d) evolution of pressure coefficient distributions.

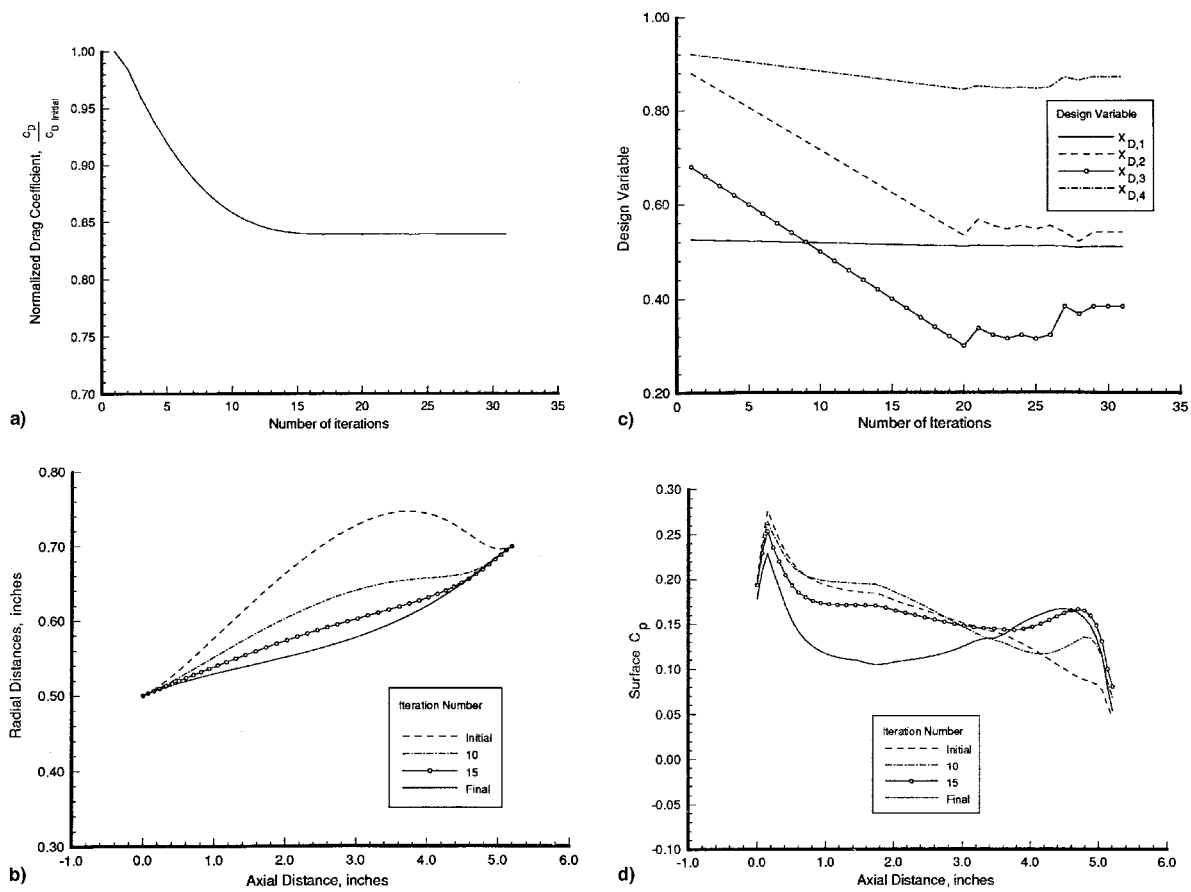

Fig. 5 Optimization of the isolated nacelle in laminar flow (case 3): a) objective function history, b) shape evolution, c) history of design variables, and d) evolution of pressure coefficient distributions.

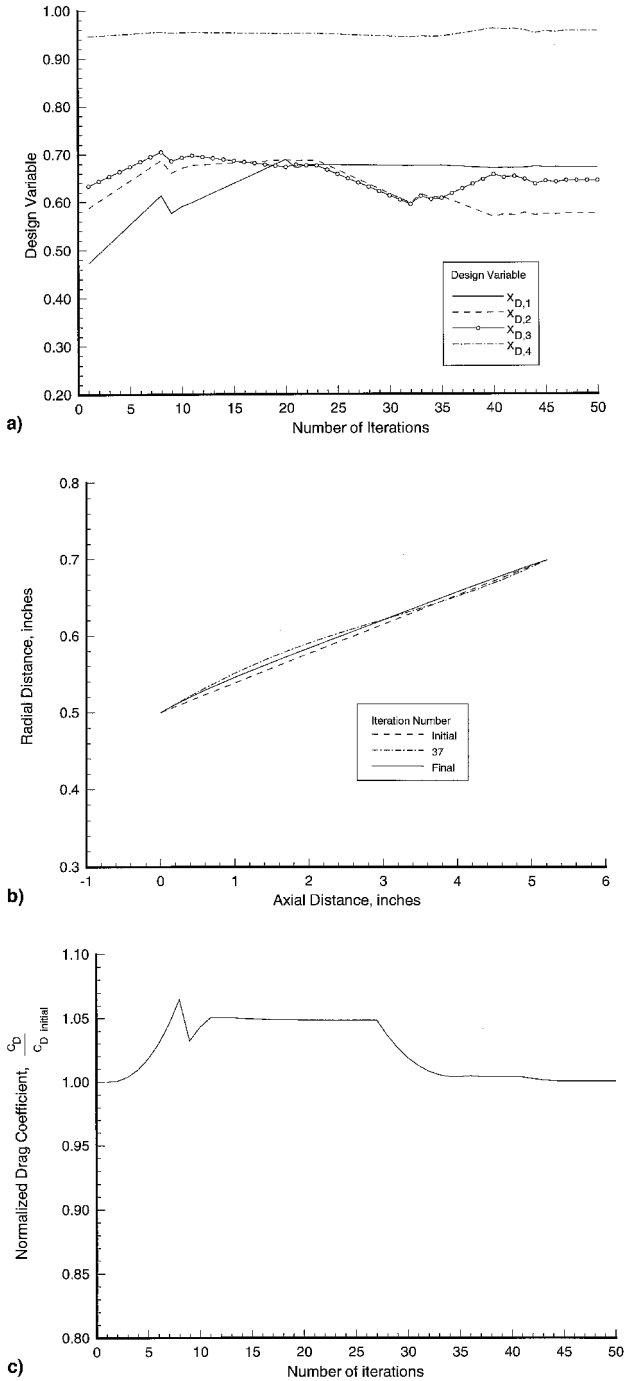

Fig. 6 Optimization of the nacelle near flat plate in inviscid flow (case 4): a) history of design variables, b) shape evolution, and c) objective function history.

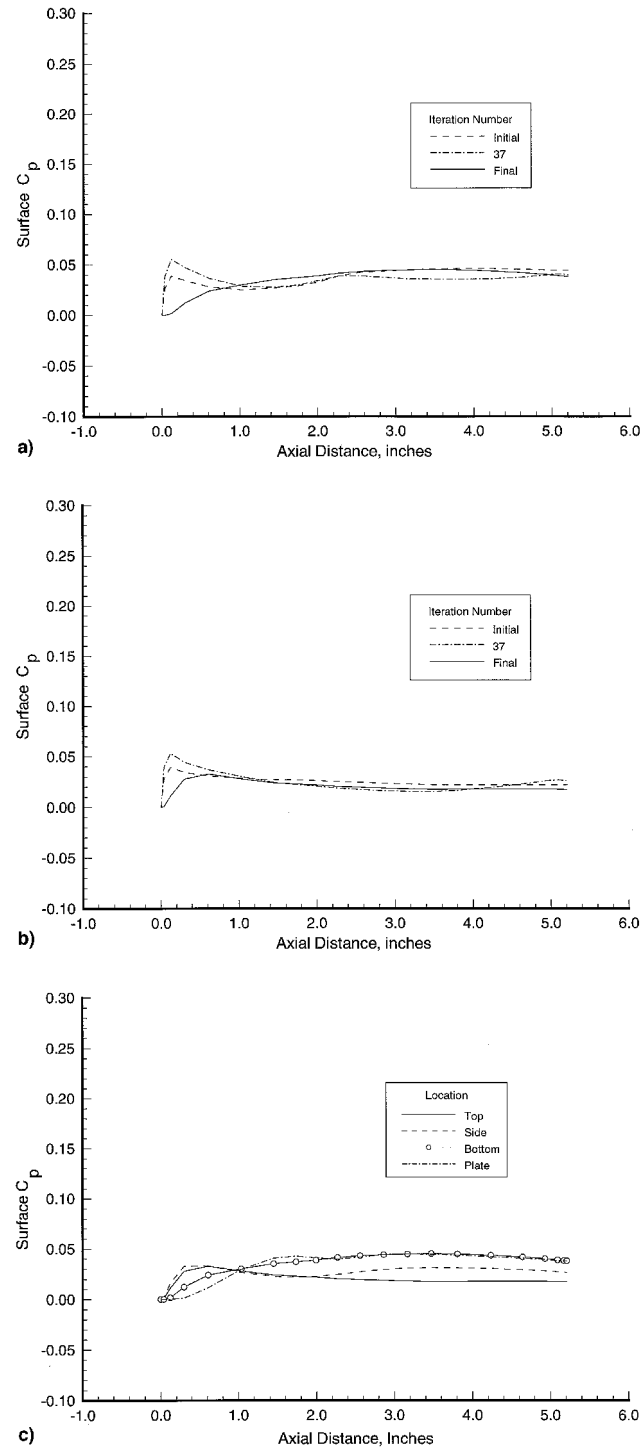

Fig. 7 Instantaneous and final pressure coefficient distributions for the nacelle near flat plate (case 4): a) on bottom of nacelle centerline (inboard), b) on top of nacelle centerline (outboard), and c) on final shape, along the top, side, and bottom of nacelle, and along the centerline of flat plate.

and the final distribution on the flat-plate are given in Figs. 7b and 7c. Again, the primary changes were realized at the lip of the nacelle. Although the shape was only varied axisymmetrically, the C_p distributions varied circumferentially because of the nonsymmetry of the flowfield (Fig. 8). The outboard flow resembled that of an isolated nacelle, but the inboard flow was clearly altered by the flat-plate interference effects, such as the shock reflected from the plate.

To scrutinize the effects of neglecting the viscosity on the shape, results of case 2 (inviscid) and case 3 (laminar) were contrasted. Furthermore, to accentuate the aerodynamic interference effects, the results of case 2 (isolated nacelle) and case 4 (nacelle near a flat-plate) were contrasted. Although the initial shapes of these cases were not similar, based on the results of cases 1 and 2, the final shapes were assumed to be only insignificantly dependent on the initial shape. The superpositions of the final shapes are presented in Fig. 9. Clearly, the inviscid assumption demonstrates a significant deviation from reality, not only in the physics of the flow, but also in the design; surprisingly, this was observed even for an isolated nacelle. Neglecting the flat-plate interference also alters the design, particularly for the first 75% of the axial length, resulting in almost a conical shape. This suggested that the conical shape in Fig. 1 was probably designed by neglecting both of these aforementioned effects; moreover, it was almost an optimum for an inviscid, non-interfering nacelle.

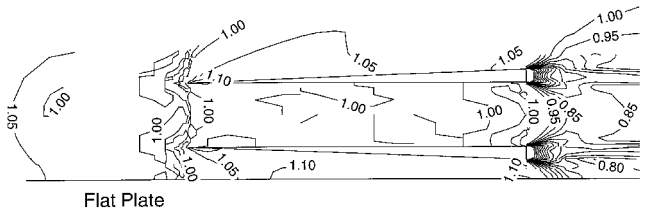

Fig. 8 Normalized density contours of the optimized nacelle near flat-plate flowfield (case 4). Plotted on the cross section A–A (see Fig. 2) and the longitudinal plane including the through-flow.

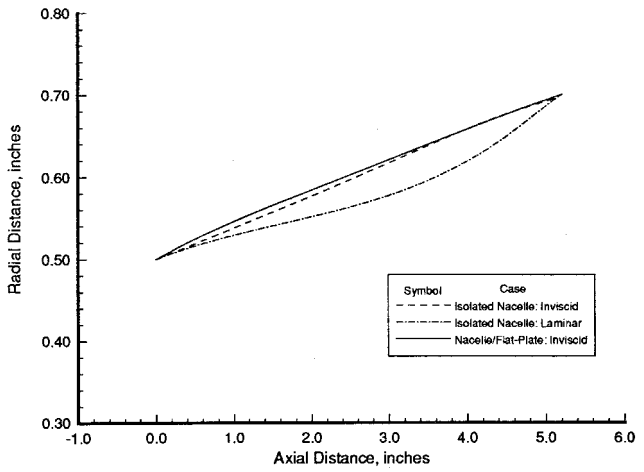

Fig. 9 Comparison of final nacelle shapes from cases 2, 3, and 4: effects of viscosity and mutual aerodynamic interference.

Finally, these optimization cases required about 240 Mbytes of memory and, depending on the number of grid blocks, the alpha-step sizes used, and the initial shape, 3–4 h of CPU time on a Cray Y-MP computer.

Conclusions

A recently developed three-dimensional, multiblock aerodynamic design optimization methodology (ADOS) was demonstrated by optimizing the shape of a nacelle model intended for a supersonic transport vehicle. The flow analysis was obtained by solving the three-dimensional, compressible, thin-layer Navier–Stokes equations or the Euler equations. The results of these simplified optimization cases offered insight into two important issues related to optimizing configurations with components in close proximity. First, accounting for the mutual aerodynamic interference between the components results in a different shape than obtained by shaping an isolated component. Secondly, the exclusion of viscous effects compromises not only the flow physics but also the optimized shapes, even for isolated components. For the specific example used in this study, it was observed that conical designs for nacelles were near optimum when interference and, more importantly, viscous effects were neglected.

The present study was primarily aimed at a methodology demonstration. To produce useful nacelle shapes of practical interest using the present methodology, the optimization problems need to be tried and recast several times to identify the best-suited objective function and constraints. For example, because the base area was not allowed to change in the present study, the base drag could improve very little. Further insight would be gained by investigating two more cases. The nacelle near the flat plate may be optimized by including the viscous effects and be contrasted with the shape of case 4. Also, the nacelle surface may be defined using a bidirectional Bezier–Bernstein representation to allow radial as well as circumferential curvature changes to produce nonaxisymmetric nacelle shapes.

Acknowledgments

This research was supported by NASA Langley Research Center, Grant NAG-1-1188. David S. Miller was the Technical Monitor. Some of the computations were performed on Numerical Aerodynamic Simulation computers. The authors thank O. J. Rose for his help.

References

[1]Welge, H. R., Radkey, R. L., and Henne, P. A., "Nacelle Integration Study on a Mach-2.2 Supersonic Cruise Aircraft," *Journal of Aircraft*, Vol. 14, No. 11, 1977, pp. 1085–1092.

[2]Robins, A. W., Morris, O. A., and Harris, R. V., "Recent Research Results in the Aerodynamics of Supersonic Vehicles," *Journal of Aircraft*, Vol. 3, No. 6, 1966, pp. 573–577.

[3]Mack, R. J., "A Numerical Method for Evaluation and Utilization of Supersonic Nacelle-Wing Interference," NASA TN D-5057, March 1969.

[4]Fouladi, K., "Viscous Flow Past a Nacelle Isolated and in Proximity of a Flat Plate," *Proceedings of 10th Applied Aerodynamics Conference* (Palo Alto, CA), AIAA, Washington, DC, 1992, pp. 919–927.

[5]Rose, O. J., "CFD Studies of Propulsion-Airframe Integration Aerodynamics for HSCT Applications," *1st NASA/Industry High-Speed Research Propulsion/Airframe Integration Workshop* (Cleveland, OH), NASA Conference Proceedings 1993, pp. 477–496.

[6]Baysal, O., and Eleshaky, M. E., "Aerodynamic Design Optimization Using Sensitivity Analysis and Computational Fluid Dynamics," *AIAA Journal*, Vol. 30, No. 3, 1992, pp. 718–725.

[7]Eleshaky, M. E., and Baysal, O., "Airfoil Shape Optimization Using Sensitivity Analysis on Viscous Flow Equations," *Journal of Fluids Engineering*, Vol. 115, No. 1, 1993, pp. 75–84.

[8]Burgreen, G. W., Baysal, O., and Eleshaky, M. E., "Improving the Efficiency of Aerodynamic Shape Optimization Procedures," *AIAA Journal*, Vol. 32, No. 1, 1994, pp. 69–76.

[9]Eleshaky, M. E., and Baysal, O., "Aerodynamic Shape Optimization via Sensitivity Analysis on Decomposed Computational Domains," *Computers and Fluids*, Vol. 23, No. 4, 1994, pp. 595–611.

[10]Eleshaky, M. E., and Baysal, O., "Preconditioned Domain Decomposition Scheme for 3-D Aerodynamic Sensitivity Analysis," *AIAA Journal*, Vol. 32, No. 12, 1994, pp. 2489–2491.

[11]Flamm, J. D., and Wilcox, F. J., Jr., "Drag Measurements of an Axisymmetric Nacelle Mounted on a Flat Plate at Supersonic Speeds," *1st NASA/Industry High-Speed Research Propulsion/Airframe Integration Workshop* (Cleveland, OH), NASA Conference Proceedings 1993, pp. 411–430.

[12]Burgreen, G. W., and Baysal, O., "Three-Dimensional Aerodynamic Shape Optimization Using Discrete Sensitivity Analysis," *AIAA Journal*, Vol. 34, No. 9, 1996, pp. 1761–1770.

[13]Vanderplaats, G. N., "An Efficient Feasible Directions Algorithm for Design Synthesis," *AIAA Journal*, Vol. 22, No. 11, 1984, pp. 1633–1640.

[14]Thomas, J. L., Krist, S. T., and Anderson, W. K., "Navier-Stokes Computations of Low Aspect Ratio Wings," *AIAA Journal*, Vol. 28, No. 2, 1990, pp. 205–215.